4904–4913 *Nucleic Acids Research, 2012, Vol. 40, No. 11* *Published online 22 February 2012*
doi:10.1093/nar/gks140

Ca^{2+} improves organization of single-stranded DNA bases in human Rad51 filament, explaining stimulatory effect on gene recombination

Louise H. Fornander[1], Karolin Frykholm[2], Anna Reymer[1], Axelle Renodon-Cornière[3], Masayuki Takahashi[3] and Bengt Nordén[1,*]

[1]Department of Chemical and Biological Engineering, Chalmers University of Technology, [2]Department of Physics, University of Gothenburg, S-41296 Gothenburg, Sweden and [3]Research Unit UMR 6204, Centre National de la Recherche Scientifique, University of Nantes, F-44322 Nantes cedex 3, France

Received December 2, 2011; Revised January 19, 2012; Accepted January 20, 2012

ABSTRACT

Human RAD51 protein (HsRad51) catalyses the DNA strand exchange reaction for homologous recombination. To clarify the molecular mechanism of the reaction *in vitro* being more effective in the presence of Ca^{2+} than of Mg^{2+}, we have investigated the effect of these ions on the structure of HsRad51 filament complexes with single- and double-stranded DNA, the reaction intermediates. Flow linear dichroism spectroscopy shows that the two ionic conditions induce significantly different structures in the HsRad51/single-stranded DNA complex, while the HsRad51/double-stranded DNA complex does not demonstrate this ionic dependence. In the HsRad51/single-stranded DNA filament, the primary intermediate of the strand exchange reaction, ATP/Ca^{2+} induces an ordered conformation of DNA, with preferentially perpendicular orientation of nucleobases relative to the filament axis, while the presence of ATP/Mg^{2+}, ADP/Mg^{2+} or ADP/Ca^{2+} does not. A high strand exchange activity is observed for the filament formed with ATP/Ca^{2+}, whereas the other filaments exhibit lower activity. Molecular modelling suggests that the structural variation is caused by the divalent cation interfering with the L2 loop close to the DNA-binding site. It is proposed that the larger Ca^{2+} stabilizes the loop conformation and thereby the protein–DNA interaction. A tight binding of DNA, with bases perpendicularly oriented, could facilitate strand exchange.

INTRODUCTION

Human RAD51 protein (HsRad51) catalyses the strand exchange reaction, which is a crucial step of homologous recombination, an evolutionary well conserved and central process of DNA metabolism. HsRad51 is thus vital for cell survival and maintenance of the genomic information by ensuring an error-free recombinational repair of double-strand breaks, the most severe DNA damage (1,2). The protein is also involved in the creation of gene diversity, shuffling homologous paternal and maternal DNA strands, as well as in cell proliferation by assisting DNA segregation (3). Both the up- and down-regulations of HsRad51 seem to relate to cancer formation (4,5). Besides its vital biological roles, the strand exchange reaction can be highly exploited in the medicinal field. It could be exploited in correction and repair of defective genes in gene therapy (6–8) and due to its relationship with cancer cell proliferation and radiotherapy resistance, it is also a potential target for anticancer treatment (9,10).

HsRad51, like its well-studied bacterial homologue RecA, catalyses the strand exchange reaction by first cooperatively assembling around single-stranded DNA (ssDNA) in the presence of ATP, forming a nucleoprotein filament in which the DNA is stretched ~50% compared with its canonical B form (11,12). This HsRad51/ssDNA filament engages a double-stranded DNA (dsDNA) with homologous sequence and promotes strand exchange between the two DNA molecules. Finally, HsRad51 is released from the newly formed dsDNA hybrid. Despite extensive studies on both HsRad51 and RecA, the molecular mechanisms involved in both the search for homologous DNA as well as the strand exchange reaction itself remain unclear (13–17). Although HsRad51 and RecA

*To whom correspondence should be addressed. Tel: +46 317723041; Fax: +46 317723858; Email: norden@chalmers.se

have functionalities in common and the overall structure of the nucleoprotein filaments they form are highly similar (12), there are some distinct differences between the two proteins. The strand exchange activity *in vitro* is much weaker for HsRad51 (18,19) and it also presents a salt dependence different from that of RecA (20–22). Interestingly, HsRad51 exhibits a more efficient strand exchange in the presence of Ca^{2+} compared with Mg^{2+}, while the strand exchange activity of RecA requires high concentration of Mg^{2+}.

It has been suggested that the different responses of HsRad51 to the two cationic conditions may be explained by the formation of a more stable and regular filament in the presence of Ca^{2+} compared with Mg^{2+} (20,23,24). Structural differences between the HsRad51/ssDNA/ATP complexes with Ca^{2+} and Mg^{2+} have also been proposed from fluorescence analysis of a DNA analogue, etheno-DNA, in complex with HsRad51 (20). The stronger fluorescence intensity from etheno-DNA in the complex with Ca^{2+} compared with the complex with Mg^{2+} may reflect differences in the organization and unstacking of the DNA bases (25–28). Also, crystallographic studies of the archaeal homologue MvRadA (22) have shown that the presence of Ca^{2+} induces a well-ordered α-helical structure of the C-terminus region of the L2 loop, one of the putative DNA binding loops (29,30). This specific conformation of the L2 loop is believed to enhance the stiffness and stability of the nucleoprotein filament. Surprisingly, with Mg^{2+} the L2 loop does not adopt a similar conformation but instead seems to be disordered, since no diffraction from the L2 loop was observed in the crystal structures of MvRadA formed in the presence of Mg^{2+} (22,30).

In an attempt to unveil the molecular mechanism behind the ion dependence of the HsRad51 strand exchange activity, we have investigated the structural variations in HsRad51/DNA complexes with different nucleotide cofactors, formed in the presence of Ca^{2+} and Mg^{2+}, using flow linear dichroism (LD) spectroscopy and molecular modelling, and then correlated the filament structures to their strand exchange activity. Flow LD is a powerful technique to determine the structure of filamentous molecules or complexes, like the HsRad51/DNA complex, in solution (32,33). The intensity of the LD signal provides information about hydrodynamic properties, such as stiffness and overall structure, while the spectral details can provide information about the orientation of specific chromophores within the molecule relative to the filament axis. This technique has been successfully used in studies of RecA/DNA and HsRad51/dsDNA complexes (34,35). From flow LD, we have previously demonstrated that the DNA bases in the complex of bacterial RecA, ssDNA and ATP are oriented nearly perpendicular to the filament axis (36), while no preferential orientation is observed in the absence of ATP. This organization of DNA bases may facilitate the search for homology and thus increase the protein strand exchange activity (16).

In the present study, we show that in the presence of ATP and Ca^{2+}, but not ATP and Mg^{2+}, ssDNA bound to HsRad51 is well ordered and the DNA bases are oriented with their planes rather perpendicular to the filament axis. Since ATP is hydrolyzed by HsRad51 during strand exchange, we have examined the nucleoprotein structure in the presence of both ATP and ADP. As RecA demonstrates a strongly reduced DNA binding capacity in the presence of ADP (37,38), the RecA/DNA/ADP filament cannot be studied. On the other hand, HsRad51 binds relatively strongly to DNA also in the presence of ADP (39), which motivated us to study also the influence of ATP/ADP in some detail.

We have finally examined the role of cations in the HsRad51 filament structure through molecular modelling. Molecular dynamics (MD) simulations demonstrate that the divalent cations stabilize an α-helical conformation of the L2 loop, which is in close contact with DNA, thus indirectly affecting the DNA binding and the whole filament structure. Also, from previously published crystal structures of MvRadA it is expected that Ca^{2+} is more tightly bound than Mg^{2+} (22). We suggest that the observed variations in structure and strand exchange activity of HsRad51 filaments, formed with either Mg^{2+} or Ca^{2+}, could be due to the fact that Ca^{2+}, being a larger ion and thus having a tighter binding and longer residence time, has a greater stabilizing effect on the L2 loop than Mg^{2+}.

MATERIALS AND METHODS

Materials

Wild-type human Rad51 protein was purified as previously described (30). Calf thymus DNA and poly(dT) were purchased from Sigma, and poly(dεA) was prepared by chemical modification of poly(dA) (Sigma) with chloroacetaldehyde (Aldrich) as described by Cazenave *et al.* (27). The concentrations of poly(dT) and calf thymus DNA were determined by ultraviolet (UV) absorption using the extinction coefficients $\varepsilon_{263\,nm} = 8520\,M^{-1}cm^{-1}$ for poly(dT) and $\varepsilon_{260\,nm} = 6600\,M^{-1}cm^{-1}$ per nucleobase for calf thymus DNA. The concentration and degree of modification of poly(dεA) were determined from the UV absorption spectrum using the formulas given by Ledneva *et al.* (40), providing $\varepsilon_{257\,nm} = 3990\,M^{-1}cm^{-1}$ and a modification degree of 93%.

The buffer used in the experiments, if not noted otherwise, contained 20 mM Tris–HCl (pH 7.5), 40 mM NaCl, 30% glycerol, 0.2 mM ethylenediaminetetraacetic acid, 0.1 mM ethyleneglycoltetraacetic acid 1.2 mM of either $MgCl_2$ or $CaCl_2$ and trace amounts of dichlorodiphenyltrichloroethane from the protein storage buffer (<60 μM).

Flow LD measurements

LD was measured on a Chirascan spectropolarimeter (Applied Photophysics). The samples were aligned using an inner rotating Couette flow cell with a total path length of 1 mm, and the shear rate was $1500\,s^{-1}$. The spectra were measured between 350 nm and 200 nm for samples containing poly(dT) and between 400 nm and 200 nm for samples containing poly(dεA) (bandwidth: 1 nm; data increment: 0.5 nm; time-per-point: 0.5 s) and four spectra

were averaged to increase the signal to noise ratio. Baseline correction was made by subtracting a spectrum measured without rotation of the Couette flow cell. The complexes were formed by mixing 4 μM HsRad51 protein, 12 μM (base) poly(dT) or poly(dεA) and 300 μM ATP or ADP in the indicated buffer. In some cases, an ATP regeneration system, consisting of 2 mM creatine phosphate and 75 μg/ml creatine kinase, was added.

Strand exchange activity

The strand exchange activity assay was performed as described by Nomme *et al.* (41) measuring the exchange between a single-stranded oligonucleotide of 58 bases and its homologous double-stranded oligonucleotide of 32 bp. Experiments were performed with 0.5 μM Rad51, 20 nM (in fragment) ssDNA, 50 nM (in fragment) dsDNA, 1 mM $CaCl_2$ or $MgCl_2$ in 20 mM Tris–HCl (pH 8), 1 mM ATP, 1 mM dichlorodiphenyltrichloroethane, 100 μg/ml bovine serum albumin and 2% glycerol.

Molecular modelling

The conformation of the L2 loop of an HsRad51 monomer, adopted from our previous filament model (30), was redesigned using a homology modelling approach followed by structural equilibration with molecular dynamics (MD). The C-terminus region of the L2 loop (residues from Gly283 to Arg293) was taken from the crystal structures of homologous ScRad51 (PDB entry 1SZP) and HsDMC1 (PDB entry 1V5W), and the rest of the loop (Val263-Gly282) was added using USCF Chimera (42). The HsRad51 monomer structure was equilibrated with MD using AMBER-f10 force fields and a standard protocol (43), details of which are given below.

A rigid body docking of ATP/ADP into the equilibrated structure of the HsRad51 monomer was performed with USCF DOCK6.5 (http://dock.compbio.ucsf.edu/). The docking analysis was based on a geometric matching algorithm and a lowest energy binding mode search. An electrostatic potential analysis was performed, in order to revise the DNA binding mode inside the protein filament, using the PDB2PQR server (44). For visualization of the results USCF Chimera was used.

All MD simulations in this study were carried out according to the following protocol: initial 1000 steps of steepest descent, followed by 1000 steps of conjugate gradient performed in explicit water (TIP3P water model) and subsequent fast heating (50 ns) to 300 K with harmonic restraints of 20 kcal/mol $Å^2$ on the heavy atoms of the solutes; restraints were then gradually removed in a series of equilibration runs of 100 ps each. MD trajectories of 20 ns at constant temperature (300 K) and pressure (1 bar), using AMBER11 software package (45,46), were recorded for a filament fragment consisting of four HsRad51 monomers gathered around a 15-base long oligo(dT) in complex with ATP or ADP, with either Mg^{2+} or Ca^{2+}. The model system was varied in terms of placement of the divalent cation (in each simulation either Ca^{2+} or Mg^{2+} was present), choice of cofactor (ATP or ADP) and whether ssDNA was present or absent inside the filament. The cations were placed in two different ways: (i) one cation (Ca^{2+}/Mg^{2+}) coordinating the ATP/ADP Pγ/Pβ-oxygens and the second cation (Ca^{2+}/Mg^{2+}) placed at the C-terminus of the L2 loop, coordinating the carboxyl groups of the protein backbone of His283–Ser285; (ii) a single cation (Ca^{2+}/Mg^{2+}), coordinating the ATP/ADP oxygens. The ssDNA fragment used in this study was adopted from the crystal structure of a RecA-ssDNA filament complex (PDB entry 3CMU) (14).

RESULTS

LD of HsRad51/ssDNA/ATP

We have measured LD of flow-oriented HsRad51/ssDNA complexes to investigate how the filament structure is influenced by the presence of Ca^{2+} and Mg^{2+}. The LD signal depends upon the macroscopic orientation of the filament and on the local orientation of the chromophores within the complex, such as DNA bases, aromatic amino acid residues and ATP. When the nucleoprotein is aligned by the shear flow, any ordered structure of chromophores will give rise to an LD signal, defined as the differential absorption between parallel and perpendicularly polarized light, respectively, $LD = A_{||} - A_{\perp}$ (33). In the LD setting used here, the filaments are preferentially aligned by the flow with their fibre axes parallel the flow and the polarization direction denoted as 'parallel'. Thus, a positive LD signal may stem from chromophores oriented with their transition moments aligned in the same direction as the filament axis ($A_{||} > A_{\perp}$), while a negative LD signal would indicate chromophores aligned more perpendicular to the filament axis ($A_{||} < A_{\perp}$). In addition, if the degree of macroscopic orientation of the filament can be determined independently, e.g. calibrated from the LD of internal standards of known orientation, LD can also provide quantitative orientation angles for the various chromophores (30,33).

Neither ssDNA nor HsRad51 alone gives rise to any significant LD signal, regardless of the presence or absence of nucleotide cofactors (results not shown). ssDNA, in contrast to dsDNA, has a flexible structure so that its bases on the whole appear unoriented even at high shear-flow gradients, while HsRad51 alone, in the concentration range used here, does not form stable, sufficiently long filaments to be significantly oriented (47). However, in combination, the HsRad51/poly(dT)/ATP complexes with Ca^{2+} as well as with Mg^{2+} exhibit relatively strong LD signals (Figure 1A), although weaker than that observed for the RecA/ poly(dT)/ATPγS complex (35). This observation indicates that HsRad51 forms quite a long and regular filament around poly(dT). If discontinuous short filaments were formed, with naked DNA regions in between, the filament stretches would act as flexible joints and the sample would not align in the shear flow, resulting in a much weaker, if any, LD signal (48). Interestingly, the formation of stiff nucleoprotein filaments, which are aligned by shear flow, requires both ATP and divalent ions. In the absence of either, we observed only weak LD signals (results not shown).

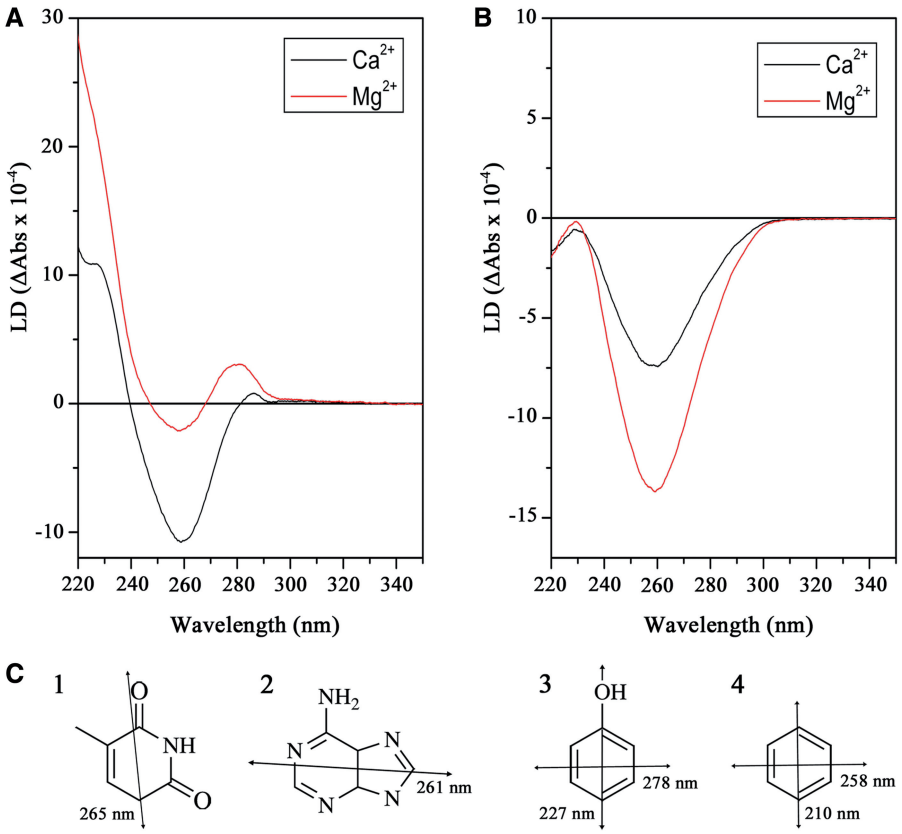

Figure 1. LD spectra of HsRad51/DNA/ATP complexes: comparison between Ca^{2+} and Mg^{2+} conditions. (**A**) Complexes were formed by mixing HsRad51, poly(dT) and ATP in buffer containing Ca^{2+} (black) or Mg^{2+} (red) as described in text. LD spectra were measured after 2 h incubation at room temperature. (**B**) Complexes were formed by mixing HsRad51 and ATP together with calf thymus DNA in the presence of Ca^{2+} (black) or Mg^{2+} (red) and incubated for 2 h before LD measurement. (**C**) Transition moments responsible for LD signals at indicated wavelengths: thymine (1), adenine (2), tyrosine (3) and phenylalanine (4).

Figure 1A shows the LD spectra of HsRad51 in complex with poly(dT) and ATP in the presence of Mg^{2+} or Ca^{2+} after 2 h incubation at room temperature. Both complexes exhibit strong LD signals, proving the formation of stiff complex, but we can also note that the shapes of the LD spectra, which are dependent on the orientation of the individual chromophores, for the Rad51/poly(dT) complexes with Ca^{2+} and Mg^{2+} differ from each other. The complex with Mg^{2+} exhibits a positive band at 280 nm and a negative band ~260 nm of similar intensity, while the complex with Ca^{2+} exhibits an intense negative band ~260 nm and a weak positive band at 285 nm. These spectral variations reveal a clear structural difference depending upon type of divalent cation. Interestingly, such a conspicuous structural difference between Mg^{2+} and Ca^{2+} conditions is not observed for the complex with dsDNA (Figure 1B). The shapes of the LD spectra of the two complexes formed with dsDNA are nearly identical, only their intensities differ. This indicates similar organization of DNA bases and HsRad51 subunits in the complex but somehow different hydrodynamic properties.

The observed LD signals in Figure 1A coincide with the absorption wavelengths for the transition moments of poly(dT) and ATP, both absorbing ~260 nm [265 nm for poly(dT) and 261 nm for ATP]. The nucleobases also absorb <230 nm, as do transition moments of the tyrosine and phenylalanine residues of HsRad51, absorbing at 227 and 278 nm, and 210 nm and 258 nm, respectively (49) (Figure 1C). Thus, absorption at wavelengths around and <230 nm could stem from a combination of transition moments in the HsRad51 filament: DNA, ATP, and tyrosine and phenylalanine residues all absorb here, as well as peptide bonds in the protein. It is therefore hard to deduce from which of these molecules the positive LD signal in this wavelength region really originates. However, the spectral variations ~260 nm observed between the complexes with Ca^{2+} and Mg^{2+} could be related to differences in either the orientation of the DNA bases or the orientation of ATP, assuming similar stiffness (hydrodynamic properties) of the two filaments. It should be noted that the strength of the LD signal cannot be directly translated into angular orientations of chromophores within the filament as these absorptions are centred very close to each other in the LD spectra (260 nm and 280 nm), and have opposite signs. The signals will therefore partly cancel each other and, in addition, the LD maxima will be shifted apart (33).

To examine whether the observed large difference at 260 nm in the LD spectra for HsRad51/ssDNA/ATP

with Ca^{2+} and Mg^{2+} is due to a corresponding difference in orientation of ATP or DNA bases, we measured LD under the same conditions, but using poly(dεA) instead of poly(dT). In poly(dεA), the adenine bases of poly(dA) are modified to 1,N6-ethenoadenine (εA), which has an additional absorption band ~310 nm (50), where no other chromophore of the HsRad51/DNA/ATP system absorbs. Thus, the LD signal >300 nm is unambiguously related to the orientation of the ssDNA bases within the nucleoprotein filament. Furthermore, the LD is not overlapped or cancelled by any other LD contributions at this wavelength, but reflects the true orientation of the modified base.

The LD spectra of HsRad51/poly(dεA)/ATP complexes with Ca^{2+} and Mg^{2+} are shown in Figure 2. We note that the LD intensity of Rad51/poly(dεA) complexes is weaker than that of HsRad51/poly(dT) complexes, suggesting that HsRad51 cannot form as long and stiff filaments on poly(dεA) as RecA (34,36). Nevertheless, the HsRad51/poly(dεA) complex with ATP/Ca^{2+} clearly shows a negative LD signal at 310 nm and another large negative signal ~225 nm (Figure 2), which also stems from the absorption of poly(dεA). The negative signal at 260 nm could originate from the absorption of poly(dεA) but also from well-oriented ATP. However, for the complex formed with ATP/Mg^{2+} no significant LD signal at 310 nm was observed (Figure 2). This demonstrates clearly that in the nucleoprotein complex with ATP/Ca^{2+} the DNA bases are structurally ordered preferentially perpendicular to the filament, while there is no such well-defined orientation of DNA bases in the complex formed with ATP/Mg^{2+}. The LD signal detected for the HsRad51/poly(dεA) complex with ATP/Mg^{2+} is therefore most likely composed of contributions only from the aromatic residues of HsRad51 and ATP. This conclusion is strongly supported by the fact that

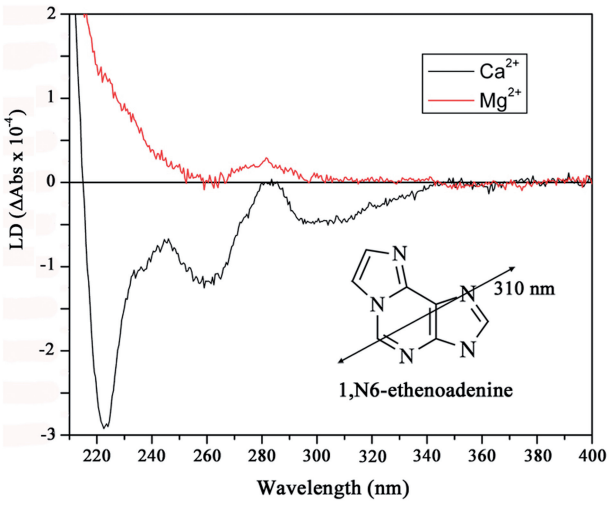

Figure 2. LD spectra of HsRad51/poly(dεA)/ATP complexes: comparison between Ca^{2+} and Mg^{2+} conditions. Complexes were formed by mixing HsRad51, poly(dεA) and ATP in the presence of Ca^{2+} (black) or Mg^{2+} (red). LD spectra were measured after 2 h incubation at room temperature. Transition moment responsible for the LD signal at 310 nm is shown in the molecular structure of 1,N6-ethenoadenine.

the shape of the LD spectra of the HsRad51/poly(dT) complex and the HsRad51/poly(dεA) complex, when formed in the presence of ATP/Mg^{2+}, are similar despite the large differences in the absorption patterns of poly(dT) and poly(dεA). Thus, the negative LD band ~260 nm of the HsRad51/poly(dT) complex with ATP/Mg^{2+} is probably due to the organization of the adenine base of ATP rather than the DNA. The binding mode of ATP in the HsRad51/ssDNA filament deduced from molecular modelling (see below) indeed suggests an orientation that would give a negative LD signal ~260 nm for either of the cationic conditions.

LD of HsRad51/ssDNA/ADP

Since the ATPase activity of HsRad51, generally weak, is significantly higher in the presence of Mg^{2+} compared with Ca^{2+} (20), we needed to verify that the structural variation between the two cationic conditions was not due to accumulation of ADP. Therefore, we first followed the variation in the LD signal for the two different complexes over time, recording spectra once every hour during 6 h and after over-night incubation. Secondly, we measured LD in the presence of an ATP regeneration system, and finally we recorded the LD spectra of the HsRad51/ssDNA complexes formed under the two different cationic conditions, but with ATP substituted for ADP.

The HsRad51/ssDNA complex with ATP/Ca^{2+} is quite stable over time, after an initial 15% increase in signal strength during the first hour the signal decreases slowly. The signal strength at 6 h is ~85% of that of the first time-point and there is only a 10% further decrease in signal strength after over-night incubation (Supplementary Figure S1). The LD signal for the complex with ATP/Mg^{2+} is also stable during the first 6 h, but greater changes appear after over-night incubation, the signal increasing by as much as 65%. This indicates that there is no significant ADP accumulation during the first hours and the observed structural variations after 2 h incubation cannot be explained merely by ADP accumulation, which is consistent with the weak ATPase activity of HsRad51 (29,51). Further support for this conclusion is the observation that the presence of an ATP regeneration system does not significantly modify the LD spectrum even after 2 h of incubation (Supplementary Figure S2). The addition of an ATP regeneration system increases the ATP concentration in solution, although we cannot still exclude the possibility that ADP is trapped inside the filament.

The LD spectra of HsRad51/poly(dT) filaments formed in the presence of ADP/Mg^{2+} and ADP/Ca^{2+} after 2 h incubation (Figure 3) display clear differences compared with the spectra of the corresponding filaments formed with ATP. As already concluded, these observed variations cannot be explained by the accumulation of ADP, or a simple conversion of the ATP-bound complex into the corresponding ADP-bound complex. The LD spectra of complexes with ADP vary between Mg^{2+} and Ca^{2+} conditions as well. Interestingly, the LD spectrum of the HsRad51/ssDNA complex with ADP/Ca^{2+} is very similar

to that of the complex formed with ATP/Mg^{2+} (during the first 6 h), suggesting that these filaments are structurally similar.

Surprisingly, the LD signal of the HsRad51/ssDNA filament with ATP/Mg^{2+} after overnight incubation differs significantly from that of the complex formed with ADP/Mg^{2+} (Supplementary Figure S3). This seems to confirm that even if some of the ATP within the filament is hydrolyzed to ADP during the long incubation time, two different structures still exist, depending on whether any ATP is present or not.

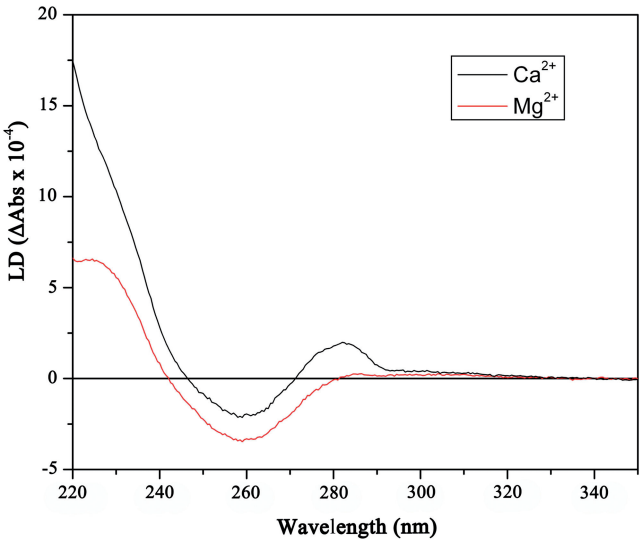

Figure 3. LD spectra of HsRad51/poly(dT)/ADP complexes. Complexes were formed by mixing HsRad51, poly(dT) and ADP in the presence of Mg^{2+} (red) or Ca^{2+} (black). LD spectra were measured after 2 h incubation at room temperature.

Correlation between structure and strand exchange activity

The strand exchange activity of HsRad51 was examined under the same conditions as in our LD study in search for a structure-function relationship. In agreement with results reported previously by Bugreev and Mazin (20), the strand exchange activity in the presence of ATP/Ca^{2+} is 2–3 times higher than that in the presence of ATP/Mg^{2+} (Figure 4). We also observed a higher strand exchange activity when the concentration of Ca^{2+} was increased to 5 mM, consistent with their results. Surprisingly, we also observed that HsRad51 exhibits some strand exchange activity in the presence of ADP/Ca^{2+}, which, according to our LD analysis, promotes a similar structure of the HsRad51/ssDNA complex as ATP/Mg^{2+}. To verify that there is no contamination of ATP or any exonuclease activity in the sample, we have performed HPLC analysis for ATP and monitored the fluorescence of poly(dεA) (results not shown). In contrast, HsRad51 does not present any significant strand exchange activity with ADP/Mg^{2+}. Obviously the structure of the HsRad51/ssDNA complex in the presence of ADP/Mg^{2+}, as judged from the LD spectrum, differs

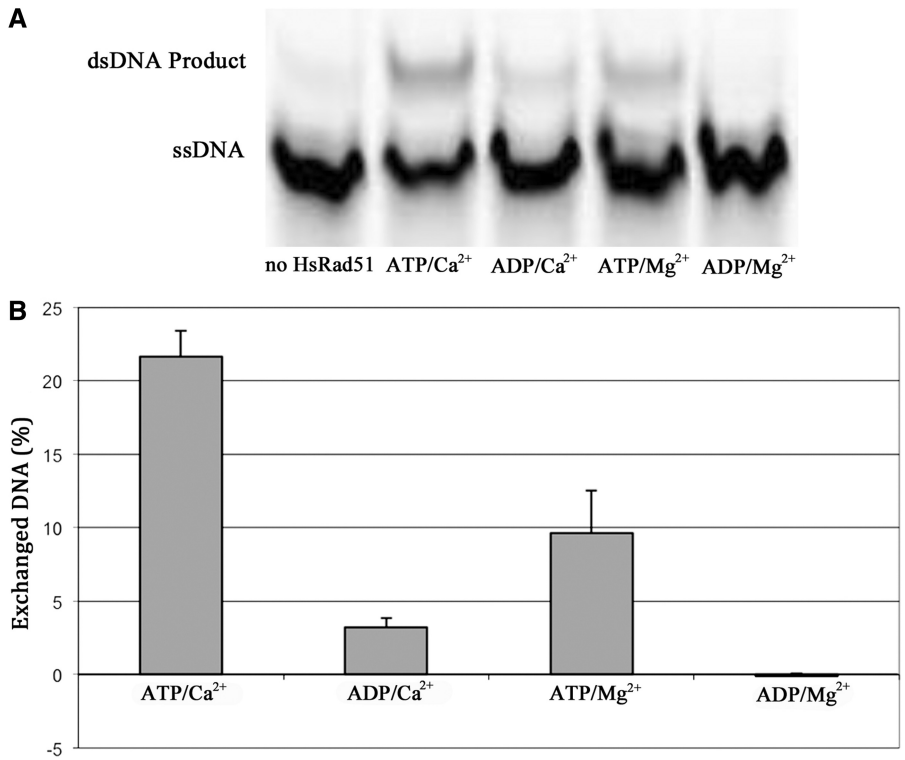

Figure 4. Effects of Ca^{2+} and Mg^{2+} ions on DNA strand exchange activity of HsRad51. HsRad51-promoted strand exchange between labelled ssDNA and the homologous dsDNA in the presence of ATP/Ca^{2+}, ATP/Mg^{2+}, ADP/Ca^{2+} or ADP/Mg^{2+} was performed as described in text. The products were separated by gel electrophoresis (**A**) and quantified (**B**).

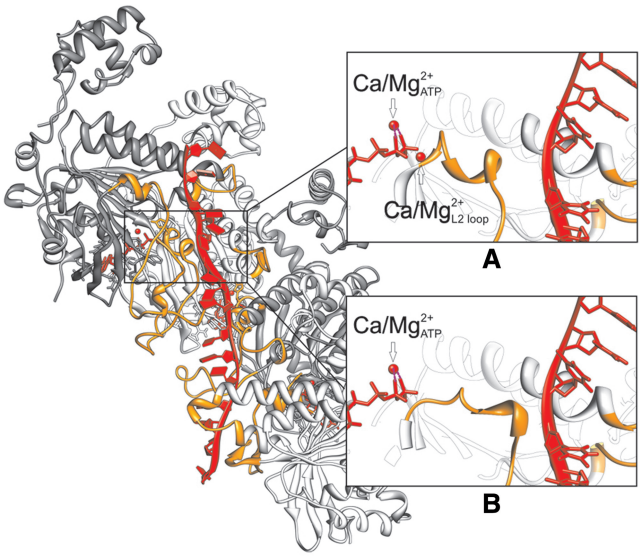

Figure 5. Model structure of the HsRad51/ssDNA/ATP filament with and without a divalent cation, (**A**) and (**B**), respectively, at the C-terminus of the L2 loop (orange). One cation (magnesium or calcium) coordinates the oxygen atoms of the phosphates of ATP (cation labelled 'ATP'), whereas another cation coordinates the α-helical region of loop L2 (cation labelled 'L2 loop'). The α-helical part of the L2 loop, which secures the DNA binding inside the nucleoprotein filament, is stable in the presence of divalent cation (Ca^{2+} or Mg^{2+}). Without one divalent ion at the C-terminus of the loop, the α-helical region becomes elongated, significantly disturbing the DNA binding.

significantly from that promoted by ATP/Mg^{2+}. In conclusion, these variations suggest that the structure of the HsRad51 filament is crucially important for its strand exchange activity.

Molecular modelling and structural analysis

To get an increased understanding of the molecular basis of the structural variations observed in LD of HsRad51/ssDNA filaments with ATP or ADP in the presence of Ca^{2+} or Mg^{2+}, we performed a molecular modelling combined with a structural analysis of the available crystal data of homologous proteins, including ScRad51 (PDB entry 1SZP), MvRadA (PDB entries 3FYH, 2I1Q, 2FPL, 1T4G and 1XU4) and HsDMC1 (PDB entry 1V5W). To this end our previous model of the protein (30) was refined. In particular, the conformation of the L2 loop was amended with the help of homology modelling using the structures of ScRad51 (PDB entry 1SZP), HsDMC1 (PDB entry 1V5W) and MvRadA (PDB entry 1XU4) as templates. The L2 loop is not only a 'host' for one Ca^{2+} or Mg^{2+} ion, but it is also positioned in close proximity to the postulated ATP/ADP binding site, the DNA-binding site and the interface between two adjacent protein monomers. The interactions and structure of the L2 loop are therefore highly relevant to this study. The final converging geometry of the L2 loop is depicted in Figure 5.

A docking analysis was carried out to find the position and orientation of ATP/ADP inside the HsRad51/ssDNA filament, with the L2 loop of the protein in a folded conformation. The binding site for ATP/ADP consists of the P-loop, which hosts the P-terminus of ATP/ADP, and the L2 loop, sequences that are highly conserved among all recombinases. Nevertheless, significant variations in their locations inside the nucleoprotein filament structure appear possible. The docking analysis placed ATP/ADP in the same binding position as that observed for the MvRadA structures (22,52), but with a slightly different orientation. This binding mode of ATP/ADP was used as a starting orientation for further simulations.

The DNA binding mode inside the HsRad51 filament was also re-examined and structurally refined. An electrostatic potential analysis of the filament structure with a redesigned L2 loop revealed the presence of a positively charged tunnel (Supplementary Figure S4) located between the two putative DNA binding loops, L1 and L2 (29). This DNA binding mode provides a better fit for the DNA helix inside the protein filament than the one suggested in our previous model (30). This binding mode of ssDNA was kept throughout further simulations.

We have performed a set of MD simulations, each 20 ns long, to examine the role of divalent cations in the nucleoprotein structure in the presence and absence of Mg^{2+} or Ca^{2+}, together with ATP or ADP. The simulations were performed with and without ssDNA in the filament. Details on model systems are given in the 'Materials and methods' section. In all simulations where the model systems had Ca^{2+} or Mg^{2+} at the C-terminus of the L2 loop, the nucleoprotein filament was stable and no significant structural changes were observed. When ssDNA was missing inside the filament, the absence of cations did not induce any structural changes, compared with a filament with cation. However, when Ca^{2+}/Mg^{2+} were absent at the C-terminus of the L2 loop and the filament contained ssDNA, the α-helical region of the L2 loop became elongated during MD (Figure 5), bringing its hydrophobic amino acid residues into the protein–DNA interaction area. This breaks the continuity of the positively charged tunnel, which provides a well-defined binding site for DNA, and loosens the protein-DNA attraction. The MD simulations with Ca^{2+} and Mg^{2+} did not show any structural divergence between the two. This could be explained by the fact that during MD simulations, the divalent ions tend to remain in their initial position, and thus no difference between Ca^{2+} and Mg^{2+} could be observed with a classic MD approach on a 20-ns time scale.

Finally, MD revealed some interesting differences in the binding mode of ATP compared with ADP. ATP sits tight in its binding pocket and the angular distribution of the electronic transition moment, which gives rise to the negative LD signal at 261 nm, varied only from 75° to 83° relative to the filament axis. For ADP, on the other hand, the binding is not as tight and the angular distribution spreads from 59° to 83°, though again contributing with a negative signal to the LD spectrum. (A pdb-formated file containing the coordinates of the model structure of the HsRad51/ssDNA/ATP/Mg^{2+} complex is available as Supplementary Dataset 1.)

DISCUSSION

To gain insight into the strand exchange reaction and to explain the molecular mechanism behind the higher activity of HsRad51 in the presence of Ca^{2+} compared with Mg^{2+}, we have investigated the structure of the first reaction intermediate, HsRad51/ssDNA/ATP (or ADP), formed in the presence of either Ca^{2+} or Mg^{2+}. Using flow-oriented samples in LD spectroscopy, we observed clear ion-dependent structural differences between the complexes with the two divalent ions in aqueous environment.

From the LD measurements on nucleoprotein filaments formed with poly(dεA), we found that the DNA bases in the complex with Ca^{2+}, the more active form, have a defined orientation. A negative LD signal at 310 nm for the complex with Ca^{2+} suggests that the bases are oriented preferentially perpendicular to the filament axis, while the complex with Mg^{2+}, the less active form, showed no signal at 310 nm, thus indicating rather randomly oriented bases. A perpendicular orientation of the bases in ssDNA may be a prerequisite for an effective strand exchange reaction, foreshadowed by base comparison and test pairing with one of the strands of the incoming dsDNA. It has previously been shown, first with LD (35) and later confirmed by a crystal structure (14), that the DNA bases in the RecA/ssDNA/ATP/Mg^{2+} complex, which has a high strand exchange activity, are also oriented with their planes approximately perpendicular to the filament axis. The lower, but still existing, strand exchange activity of HsRad51/ssDNA/ATP/Mg^{2+} could be explained by the nucleobases not being ordered in the filament. This lack of orientation of the DNA bases in the HsRad51/ssDNA/ATP/Mg^{2+} complex seen with our LD analysis cannot be explained by accumulation of ADP due to rapid ATP hydrolysis in the presence of Mg^{2+}, since the presence of an ATP regeneration system did not modify the LD signal.

The fact that the HsRad51/ssDNA/ATP filament with Mg^{2+} exhibited a significant LD signal, despite that the DNA bases are poorly aligned in the filament, indicates that HsRad51 covers ssDNA rather regularly, forming a stiff linear filament. However, the LD intensity of the HsRad51/poly(dεA)/ATP complexes was weaker than that of the HsRad51/poly(dT)/ATP complexes, both with Ca^{2+} and Mg^{2+}. This may reflect an incomplete or unstable assembly of HsRad51 on some ssDNA sequences. Such a behaviour could be a contributing explanation to the weak strand exchange activity of HsRad51 compared with that of RecA.

Our observations suggest that Ca^{2+} and Mg^{2+} influence the organization of the protein filament around ssDNA differently. To more clearly understand the structural circumstances, the two cations may impose on the overall structure of the HsRad51/ssDNA/ATP complex, we have refined our previous molecular model of the HsRad51 nucleoprotein filament (30). The conformation of the putative DNA binding loop (L2) was recalculated, providing an alternative even more favourable binding mode for DNA in a well-defined positively charged tunnel formed between the L1 and L2 loops. The conducted MD experiments reveal a delicate balance of the α-helical region stability of the L2 loop. With a divalent cation present at the loop's C-terminus, the α-helical region that interacts with the DNA backbone *via* two positively charged residues remains stable. However, when a cation is missing, the α-helical region becomes elongated, bringing its hydrophobic side chain residues close to the DNA backbone, thus significantly perturbing the protein–DNA interaction. Although MD does not show any significant differences between the simulations with Ca^{2+} and Mg^{2+}, we may argue that Mg^{2+}, being a smaller ion, may have greater mobility and less chance to reside for a long time at the C-terminus of the L2 loop, which would resemble the MD case with no cation at the C-terminus. On the other hand, for Ca^{2+}, a bigger and more massive cation, the residence time would be longer. It is worth mentioning that the region where the C-terminus of the L2 loop is located is structurally crowded, which would make it easier for the smaller Mg^{2+} ion to leave. Supporting our hypothesis is the fact that in the crystal structures of the homologous MvRadA protein, the L2 loop remains disordered in all cases when crystallization was made in the presence of Mg^{2+} (22), while when Ca^{2+} was present, the L2 loop contained an α-helical region.

It is interesting to note that the different HsRad51/ssDNA filament structures induced by Ca^{2+} and Mg^{2+} are also highly dependent on whether ATP or ADP is bound. Our MD simulations suggest that the ATP is bound more tightly in the filament than ADP and previous FRET measurements and single molecule studies indicate that the complex with ATP is stretched while that with ADP is not (51,53). Surprisingly, according to our LD analysis, the structure of the HsRad51/ssDNA/ATP/Mg^{2+} filament is similar to that of the HsRad51/ssDNA/ADP/Ca^{2+} complex, but the ATP-dependent strand exchange activity of HsRad51 is higher in the presence of ATP/Mg^{2+} than with ADP/Ca^{2+}. With ADP/Mg^{2+}, a filament stiff enough to give an LD signal is formed, but it adopts a different structure and it does not exhibit any significant strand exchange activity.

Both Ca^{2+} as well as Mg^{2+} are ubiquitous modulators of various cell functions. The total concentration of Mg^{2+} varies between cell types, but it ranges from 5 mM to 30 mM, while the free Mg^{2+} concentration has been most often determined to be around 0.4–0.6 mM (54). On the other hand, the concentration of Ca^{2+} *in vivo* does not exceed 5–10 μM and thus appears too low to stimulate homologous recombination in the cell (55). Nevertheless, it has been observed that Ca^{2+} plays an important role during the early stages of meiosis (56,57) and in response to DNA damage (58,59). It is possible that the effect we have observed *in vitro* with Ca^{2+} for the HsRad51/poly(dT) complex can also occur *in vivo* with the assistance of activator proteins.

While the HsRad51/ssDNA filament, which is the initial complex in the strand exchange reaction, is highly dependent on the divalent cation present, the HsRad51 complex formed with dsDNA does not exhibit this dependence. Our LD analysis reveals that the HsRad51/dsDNA complex forms stiff and stable filaments of similar structure with both Ca^{2+} and Mg^{2+}. Moreover, previous kinetic analyses have shown that the association and dissociation of the HsRad51/dsDNA complex are independent of the

type of divalent ions, while these processes with ssDNA depend on the ions present (23). In further support of the hypothesis that there are significant differences in the binding modes of HsRad51 to ssDNA or dsDNA, Kurumizaka *et al.* have reported that the strand exchange inhibitor halenaquinone prevents the binding of HsRad51 to dsDNA but only slightly to ssDNA (60). In the case of RecA, we have observed that the filament structure is very similar to complexes formed with ssDNA and dsDNA (61), but from this study we can definitely conclude that there are major differences in the case of HsRad51. We can also conclude that there is a clear cation dependence for both structure and activity of the HsRad51/ssDNA filament. This is probably due to the divalent cation directly affecting the protein–DNA interaction, thus exerting changes on the structure and stability of the whole filament.

SUPPLEMENTARY DATA

Supplementary Data are available at NAR Online: Supplementary Figures 1–4 and Supplementary Dataset 1.

ACKNOWLEDGEMENTS

We thank H. Hayakawa and R. Ito (Fukuoka Dental College, Fukuoka, Japan) for verifying the absence of contaminating ATP in the strand exchange reaction with ADP.

FUNDING

King Abdullah University of Science and Technology Grant (KUK-11-008-23 to L.H.F., K.F. and A.R.); European Research Council (ERC-2008-AdG 227700 to B.N.); Agence Nationale de la Recherche Grant (ANR-2010-BLAN-1013 DynRec to A.R.-C. and M.T.); BiogenOuest to A.R.-C. and M.T. Funding for open access charge: Chalmers Library.

Conflict of interest statement. None declared.

REFERENCES

1. Vispé,S., Cazaux,C., Lesca,C. and Defais,M. (1998) Overexpression of Rad51 protein stimulates homologous recombination and increases resistance of mammalian cells to ionizing radiation. *Nucleic Acids Res.*, **26**, 2859–2864.
2. Sonoda,E., Sasaki,M.S., Buerstedde,J.M., Bezzubova,O., Shinohara,A., Ogawa,H., Takata,M., Yamaguchi-Iwai,Y. and Takeda,S. (1998) Rad51-deficient vertebrate cells accumulate chromosomal breaks prior to cell death. *EMBO J.*, **17**, 598–608.
3. Tsuzuki,T., Fujii,Y., Sakumi,K., Tominaga,Y., Nakao,K., Sekiguchi,M., Matsushiro,A., Yoshimura,Y. and Morita,T. (1996) Targeted disruption of the Rad51 gene leads to lethality in embryonic mice. *Proc. Natl Acad. Sci. USA*, **93**, 6236–6240.
4. Richardson,C., Stark,J.M., Ommundsen,M. and Jasin,M. (2004) Rad51 overexpression promotes alternative double-strand break repair pathways and genome instability. *Oncogene*, **23**, 546–553.
5. Maacke,H., Opitz,S., Jost,K., Hamdorf,W., Henning,W., Krüger,S., Feller,A.C., Lopens,A., Diedrich,K., Schwinger,E. *et al.* (2000) Over-expression of wild-type Rad51 correlates with histological grading of invasive ductal breast cancer. *Int. J. Cancer*, **88**, 907–913.
6. Kowalczykowski,S.C. and Zarling,D.A. (1995) The synergistic interaction between RecA protein and SSB protein during DNA strand exchange. *Gene Targeting (Ed Vega)*. CRC press, pp. 167–210.
7. Liu,L., Maguire,K.K. and Kmiec,E.B. (2004) Genetic re-engineering of Saccharomyces cerevisiae RAD51 leads to a significant increase in the frequency of gene repair in vivo. *Nucleic Acids Res.*, **32**, 2093–2101.
8. Klug,A. (2010) The discovery of zinc fingers and their development for practical applications in gene regulation and genome manipulation. *Q. Rev. Biophys.*, **43**, 1–21.
9. Ito,M., Yamamoto,S., Nimura,K., Hiraoka,K., Tamai,K. and Kaneda,Y. (2005) Rad51 siRNA delivered by HVJ envelope vector enhances the anti-cancer effect of cisplatin. *J. Gene Med.*, **7**, 1044–1052.
10. Ohnishi,T., Taki,T., Hiraga,S., Arita,N. and Morita,T. (1998) In vitro and in vivo potentiation of radiosensitivity of malignant gliomas by antisense inhibition of the RAD51 gene. *Biochem. Biophys. Res. Commun.*, **245**, 319–324.
11. Yu,X., Jacobs,S.A., West,S.C., Ogawa,T. and Egelman,E.H. (2001) Domain structure and dynamics in the helical filaments formed by RecA and Rad51 on DNA. *Proc. Natl Acad. Sci. USA*, **98**, 8419–8424.
12. Ogawa,T., Yu,X., Shinohara,A. and Egelman,E.H. (1993) Similarity of the yeast RAD51 filament to the bacterial RecA filament. *Science*, **259**, 1896–1899.
13. Masuda,T., Ito,Y., Terada,T., Shibata,T. and Mikawa,T. (2009) A non-canonical DNA structure enables homologous recombination in various genetic systems. *J. Biol. Chem.*, **284**, 30230–30239.
14. Chen,Z., Yang,H. and Pavletich,N.P. (2008) Mechanism of homologous recombination from the RecA-ssDNA/dsDNA structures. *Nature*, **453**, 489–484.
15. Saladin,A., Amourda,C., Poulain,P., Férey,N., Baaden,M., Zacharias,M., Delalande,O. and Prévost,C. (2010) Modeling the early stage of DNA sequence recognition within RecA nucleoprotein filaments. *Nucleic Acids Res.*, **38**, 6313–6323.
16. Prévost,C. and Takahashi,M. (2003) Geometry of the DNA strands within the RecA nucleofilament: role in homologous recombination. *Q. Rev. Biophys.*, **36**, 429–453.
17. Xiao,J., Lee,A.M. and Singleton,S.F. (2006) Direct evaluation of a kinetic model for RecA-mediated DNA-strand exchange: the importance of nucleic acid dynamics and entropy during homologous genetic recombination. *Chembiochem*, **7**, 1265–1278.
18. Baumann,P., Benson,F.E. and West,S.C. (1996) Human Rad51 protein promotes ATP-dependent homologous pairing and strand transfer reactions in vitro. *Cell*, **87**, 757–766.
19. Gupta,R.C., Bazemore,L.R., Golub,E.I. and Radding,C.M. (1997) Activities of human recombination protein Rad51. *Proc. Natl Acad. Sci. USA*, **94**, 463–468.
20. Bugreev,D.V. and Mazin,A.V. (2004) Ca2+ activates human homologous recombination protein Rad51 by modulating its ATPase activity. *Proc. Natl Acad. Sci. USA*, **101**, 9988–9993.
21. Lee,M.H., Chang,Y.C., Hong,E.L., Grubb,J., Chang,C.S., Bishop,D.K. and Wang,T.F. (2005) Calcium ion promotes yeast Dmc1 activity via formation of long and fine helical filaments with single-stranded DNA. *J. Biol. Chem.*, **280**, 40980–40984.
22. Qian,X., He,Y., Ma,X., Fodje,M.N., Grochulski,P. and Luo,Y. (2006) Calcium stiffens archaeal Rad51 recombinase from Methanococcus voltae for homologous recombination. *J. Biol. Chem.*, **281**, 39380–39387.
23. Miné,J., Disseau,L., Takahashi,M., Cappello,G., Dutreix,M. and Viovy,J.-L. (2007) Real-time measurements of the nucleation, growth and dissociation of single Rad51-DNA nucleoprotein filaments. *Nucleic Acids Res.*, **35**, 7171–7187.
24. Ristic,D., Modesti,M., van der Heijden,T., van Noort,J., Dekker,C., Kanaar,R. and Wyman,C. (2005) Human Rad51 filaments on double- and single-stranded DNA: correlating regular and irregular forms with recombination function. *Nucleic Acids Res.*, **33**, 3292–3302.
25. Baker,B.M., Vanderkool,J. and Kallenbach,N.R. (1978) Base stacking in A fluorescent dinucleoside monophosphate: εApεA. *Biopolymers*, **17**, 1361–1372.

26. Tolman,G.L., Barrio,J.R. and Leonard,N.J. (1974) Chloroacetaldehyde-modified dinucleoside phosphates. Dynamic fluorescence quenching and quenching due to intramolecular complexation. *Biochemistry*, **13**, 4869–4878.
27. Cazenave,C., Toulmé,J.J. and Hélène,C. (1983) Binding of RecA protein to single-stranded nucleic acids: spectroscopic studies using fluorescent polynucleotides. *EMBO J.*, **2**, 2247–2251.
28. Chabbert,M., Lami,H. and Takahashi,M. (1991) Cofactor-induced orientation of the DNA bases in single-stranded DNA complexed with RecA protein. A fluorescence anisotropy and time-decay study. *J. Biol. Chem.*, **266**, 5395–5400.
29. Matsuo,Y., Sakane,I., Takizawa,Y., Takahashi,M. and Kurumizaka,H. (2006) Roles of the human Rad51 L1 and L2 loops in DNA binding. *FEBS J.*, **273**, 3148–3159.
30. Reymer,A., Frykholm,K., Morimatsu,K., Takahashi,M. and Nordén,B. (2009) Structure of human Rad51 protein filament from molecular modeling and site-specific linear dichroism spectroscopy. *Proc. Natl Acad. Sci. USA*, **106**, 13248–13253.
31. Wu,Y., He,Y., Moya,I.A., Qian,X. and Luo,Y. (2004) Crystal structure of archaeal recombinase RADA: a snapshot of its extended conformation. *Mol. Cell*, **15**, 423–435.
32. Nordén,B., Kubista,M. and Kuruscev,T. (1992) Linear dichroism spectroscopy of nucleic acids. *Quart. Rev. Biophys.*, **25**, 51–170.
33. Nordén,B., Rodger,A. and Dafforn,T. (2010) *Linear Dichroism and Circular Dichroism: A Textbook on Polarized Light Spectroscopy*. The Royal Society of Chemistry, Cambridge, UK.
34. Morimatsu,K., Takahashi,M. and Nordén,B. (2002) Arrangement of RecA protein in its active filament determined by polarized-light spectroscopy. *Proc. Natl Acad. Sci. USA*, **99**, 11688–11693.
35. Takahashi,M., Kubista,M. and Nordén,B. (1987) Linear dichroism study of RecA-DNA complexes. Structural evidence and binding stoichiometries. *J. Biol. Chem.*, **262**, 8109–8111.
36. Nordén,B., Elvingson,C., Kubista,M., Sjöberg,B., Ryberg,H., Ryberg,M., Mortensen,K. and Takahashi,M. (1992) Structure of RecA-DNA complexes studied by combination of linear dichroism and small-angle neutron scattering measurements on flow-oriented samples. *J. Mol. Biol.*, **226**, 1175–1191.
37. Chabbert,M., Cazenave,C. and Hélène,C. (1987) Kinetic studies of recA protein binding to a fluorescent single-stranded polynucleotide. *Biochemistry*, **26**, 2218–2225.
38. Menetski,J.P. and Kowalczykowski,S.C. (1985) Interaction of recA protein with single-stranded DNA. Quantitative aspects of binding affinity modulation nucleotide cofactors. *J. Mol. Biol.*, **181**, 281–295.
39. Kim,H.K., Morimatsu,K., Nordén,B., Ardhammar,M. and Takahashi,M. (2002) ADP stabilizes the human Rad51-single stranded DNA complex and promotes its DNA annealing activity. *Genes Cells*, **7**, 1125–1134.
40. Ledneva,R.K., Razjivin,A.P. and Bogdanov,A.A. (1978) Interaction of tobacco mosaic virus protein with synthetic polynucleotides containing a fluorescent label: optical properties of poly(A,epsilonA) and poly(C,epsilonC) copolymers and energy migration from the tryptophan to 1,N6-ethenoadenine or 3,N4-etheno. *Nucleic Acids Res.*, **5**, 4225–4243.
41. Nomme,J., Takizawa,Y., Martinez,S.F., Renodon-Cornière,A., Fleury,F., Weigel,P., Yamamoto,K., Kurumizaka,H. and Takahashi,M. (2008) Inhibition of filament formation of human Rad51 protein by a small peptide derived from the BRC-motif of the BRCA2 protein. *Genes Cells*, **13**, 471–481.
42. Pettersen,E.F., Goddard,T.D., Huang,C.C., Couch,G.S., Greenblatt,D.M., Meng,E.C. and Ferrin,T.E. (2004) UCSF Chimera–a visualization system for exploratory research and analysis. *J. Comput. Chem.*, **25**, 1605–1612.
43. Hornak,V., Abel,R., Okur,A., Strockbine,B., Roitberg,A. and Simmerling,C. (2006) Comparison of multiple amber force fields and development of improved protein backbone parameters. *Proteins*, **65**, 712–725.
44. Dolinsky,T.J., Czodrowski,P., Li,H., Nielsen,J.E., Jensen,J.H., Klebe,G. and Baker,N.A. (2007) PDB2PQR: expanding and upgrading automated preparation of biomolecular structures for molecular simulations. *Nucleic Acids Res.*, **35**, W522–W525.
45. Pearlman,D.A., Case,D.A., Caldwell,J.W., Ross,W.S., Cheatham,T.E., Debolt,S., Ferguson,D., Seibel,G. and Kollman,P. (1995) AMBER, a package of computer programs for applying molecular mechanics, normal mode analysis, molecular dynamics and free energy calculations to simulate the structural and energetic properties of molecules. *Comput. Phys. Commun.*, **91**, 1–41.
46. Case,D.A., Cheatham,T.E., Darden,T., Gohlke,H., Luo,R., Merz,K.M., Onufriev,A., Simmerling,C., Wang,B. and Woods,R.J. (2005) The Amber biomolecular simulation programs. *J. Comput. Chem.*, **26**, 1668–1688.
47. Yoshioka,K., Yumoto-Yoshioka,Y., Fleury,F. and Takahashi,M. (2003) pH- and salt-dependent self-assembly of human Rad51 protein analyzed as fluorescence resonance energy transfer between labeled proteins. *J. Biochem.*, **133**, 593–597.
48. Kim,S.K., Nielsen,P.E., Egholm,M., Buchardt,O., Berg,R.H. and Nordén,B. (1993) Right-handed triplex formed between peptide nucleic acid PNA-T8 and Poly(dA) shown by linear dichroism and circular dichroism spectroscopy. *J. Am. Chem. Soc.*, **115**, 6477–6481.
49. Sreerama,N., Manning,M.C., Powers,M.E., Zhang,J.X., Goldenberg,D.P. and Woody,R.W. (1999) Tyrosine, phenylalanine, and disulfide contributions to the circular dichroism of proteins: circular dichroism spectra of wild-type and mutant bovine pancreatic trypsin inhibitor. *Biochemistry*, **38**, 10814–10822.
50. Holmén,A., Albinsson,B. and Nordcn,B. (1994) Electronic transition dipole moments of the 1 p-ethenoadenine chromophore. *J. Phys. Chem.*, **94**, 13460–13469.
51. Renodon-Cornière,A., Takizawa,Y., Conilleau,S., Tran,V., Iwai,S., Kurumizaka,H. and Takahashi,M. (2008) Structural analysis of the human Rad51 protein-DNA complex filament by tryptophan fluorescence scanning analysis: transmission of allosteric effects between ATP binding and DNA binding. *J. Mol. Biol.*, **383**, 575–587.
52. Qian,X., Wu,Y., He,Y. and Luo,Y. (2005) Crystal structure of Methanococcus voltae RadA in complex with ADP: hydrolysis-induced conformational change. *Biochemistry*, **44**, 13753–13761.
53. Hilario,J., Amitani,I., Baskin,R.J. and Kowalczykowski,S.C. (2009) Direct imaging of human Rad51 nucleoprotein dynamics on individual DNA molecules. *Proc. Natl Acad. Sci. USA*, **106**, 361–368.
54. Hartwig,A. (2001) Role of magnesium in genomic stability. *Mutat. Res.*, **475**, 113–121.
55. Hyrc,K., Handran,S.D., Rothman,S.M. and Goldberg,M.P. (1997) Ionized intracellular calcium concentration predicts excitotoxic neuronal death: observations with low-affinity fluorescent calcium indicators. *J. Neurosci.*, **17**, 6669–6677.
56. Carroll,J., Swann,K., Whittingham,D. and Whitaker,M. (1994) Spatiotemporal dynamics of intracellular [Ca2+]i oscillations during the growth and meiotic maturation of mouse oocytes. *Development*, **120**, 3507–3517.
57. Whitaker,M. (2006) Calcium at fertilization and in early development. *Physiol. Rev.*, **86**, 25–88.
58. Popescu,R., Heiss,E.H., Ferk,F., Peschel,A., Knasmueller,S., Dirsch,V.M., Krupitza,G. and Kopp,B. (2011) Ikarugamycin induces DNA damage, intracellular calcium increase, p38 MAP kinase activation and apoptosis in HL-60 human promyelocytic leukemia cells. *Mutat. Res.*, **709–710**, 60–66.
59. Schieven,G.L., Kirihara,J.M., Burg,D.L., Geahlen,R.L. and Ledbetter,J.A. (1993) p72syk tyrosine kinase is activated by oxidizing conditions that induce lymphocyte tyrosine phosphorylation and Ca2+ Signals. *J. Biol. Chem.*, **268**, 16688–16692.
60. Takaku,M., Kainuma,T., Ishida-Takaku,T., Ishigami,S., Suzuki,H., Tashiro,S., van Soest,R.W., Nakao,Y. and Kurumizaka,H. (2011) Halenaquinone, a chemical compound that specifically inhibits the secondary DNA binding of RAD51. *Genes Cells*, **16**, 427–436.
61. Frykholm,K., Morimatsu,K. and Nordén,B. (2006) Conserved conformation of RecA protein after executing the DNA strand-exchange reaction. A site-specific linear dichroism structure study. *Biochemistry*, **45**, 11172–11178.